Sub-nanometer Wavelength Metrology of Lithographically Prepared Structures: A Comparison of Neutron and X-ray Scattering

Ronald L. Jones[a],*, Tengjiao Hu[a], Eric K. Lin[a], Wen-li Wu[a], Diego M. Casa[b], Ndubuisi G. Orji[c], Theodore V. Vorburger[c], Patrick J. Bolton[d], George Barclay[d]
[a)]NIST Polymers Division, Gaithersburg, MD 20899
[b)]Advanced Photon Source, Argonne National Laboratory, Argonne, IL 60439
[c)]NIST Precision Engineering Division, Gaithersburg, MD 20899
[d)]Shipley Company, Marlborough, MA 01752

ABSTRACT

The challenges facing current dimensional metrologies based on scanning electron microscopy (SEM), atomic force microscopy (AFM), and light scatterometry for technology nodes of 157 nm imaging and beyond may require the development of new metrologies. We provide results of initial tests of a measurement technique based on Small Angle X-ray Scattering (SAXS) capable of rapid measurements of test samples produced using conventional test masks without significant sample preparation. Using a sample photoresist grating, the technique is shown to apply to both organic, including photoresist, and inorganic patterns, including metal and oxide. The sub-Angstrom wavelength provides nanometer level resolution, with significant room for increased resolution. SAXS provides a dramatic improvement over the use of small angle neutron scattering (SANS) in measurement resolution. An additional advantage is the potential of developing a SAXS-based metrology tool on a laboratory scale.

Keywords: CD Metrology, X-ray scattering, sub-100 nm lithography

1. INTRODUCTION

With the emergence of photolithographic processing using wavelengths less than 193 nm, mass production of sub-100 nm features will require further refinement of metrology tools. The International Technology Roadmap for Semiconductors (ITRS) suggests the need for dimensional control of features on the order of a nanometer within four years. Their goal presents significant challenges to metrologies based on scanning electron microscopy (SEM), atomic force microscopy (AFM), and electrical line width (ECD).[1-4] SEM and AFM offer the advantage of real space imaging of arbitrary shapes. This capability is especially useful in the limit of non-repeating patterns or locating low concentrations of defects such as voids. For dense structures of repeating patterns, however, microscope techniques face challenges in the sub-100 nm regime due to probe size, as in the case of AFM, and the complex interaction between the probe and the patterns in the case of SEM.[2] For repeating structures, light scatterometry has emerged as the primary candidate for rapid line shape metrology. The primary challenge of light scatterometry is the significant modeling required to extract the line shape.[5,6] This is due in part to the large wavelength of the probing beam relative to the size of the structures that prohibits the measurement of valuable information obtained from diffraction. Given a library of solved models, light scatterometry is readily applied to surface structures with well-defined indices of refraction. However, changes in the material components require determinations of precise indices of refraction. In addition, structures embedded in materials of low transparency are difficult to probe. This restricts measures of embedded structures often found in, for instance, copper interconnects within a low-k dielectric matrix. To address these latter concerns, and provide additional support for microscopic imaging, we are developing a high-resolution technique based on the transmission scattering of x-rays. In this report, we provide initial results from a series of SAXS measurements of a test photoresist grating. Measurements using this technique are directly compared to an analogous set of measurements made previously using small angle neutron scattering (SANS).

The requirements of a new metrology technique include the ability for rapid measurement, minimal sample preparation, and a probe size smaller than typical test pattern arrays. Beyond these minimal requirements, other advantages are gained by applicability to a wide range of patterns, including isolated and dense lines or contact holes, as well as structures of different materials, including polymer-based photoresists, oxides, nitrides, and metals. Recognizing the advantages of a sub-nanometer wavelength and a large depth of penetration, a wide range of x-ray based techniques are

used to measure patterns in research applications.[7-14] Since many of these techniques operate in reflection, they often suffer from the requirement of large sample sizes and long data collection times.[8] In addition, the lack of a general analytical description of reflection scattering by x-rays often results in extensive modeling during data analysis.[9,10] One technique that potentially avoids the need for large samples is based on crystal truncation rod (CTR) scattering, where information on the pattern is obtained by scanning the region around a Bragg diffraction of the underlying substrate.[11-14] Using this technique, more than 20 orders of diffraction have been reported for line patterns etched in a variety of inorganic substrates.[12] The primary disadvantage of these techniques is their dependence on a highly ordered substrate to produce the Bragg reflection.

In this publication, we provide results from a new metrology technique based on small angle x-ray scattering (SAXS) that meets many of these requirements and offers resolution capabilities that meet the ITRS goal for at least the next two technology nodes. We employ a transmission scattering geometry to measure pattern shape and quality (see figure 1). Measurements performed in transmission offer several advantages, including simplification of data analysis and the general application to a wide range of ordered and amorphous substrates. The use of a 2-dimensional detector allows simultaneous data collection over a wide range of scattering vectors, providing a platform for rapid measurements. The SAXS-based technique is compared to similar efforts performed using small angle neutron scattering (SANS).[15] While each technique provides similar information, the commercial availability of x-ray sources provide the potential of exportability to industrial environments. Initially, however, the flexibility in wavelength and optics offered by a synchrotron source make it ideal for technique development. Finally, we provide initial results from a comparison of SAXS, SANS, and AFM on identical samples.

2. EXPERIMENTAL

Samples were created using conventional photolithographic processing of three different photoresist formulations. Each resist formulation was imaged at its optimal imaging conditions using the same exposure mask (figure 2). The estimated pattern is a series of photoresist lines with 1:2 spacing and a nominal repeat distance, or pitch, of ≈540 nm. The resulting line width is expected to be ≈180 nm. Photoresist gratings were produced with a repeating pattern spanning approximately 1 cm^2.

SAXS measurements were performed at the 9ID beamline of the Advanced Photon Source at Argonne National Laboratory. The optical configuration included two focusing mirrors aligned along orthogonal axes, monochromator, and two beam-defining slits with a third slit to remove parasitic scattering before the sample. Scattered intensity, I(q), where $q=4\pi/\lambda \sin(\theta)$, λ is the wavelength, and 2θ is the scattering angle measured relative to the beam center, is recorded on a 2-D CCD placed at a distance of [543 ± 2] cm from the sample.[16] The optical components are used to define a beam spot size on the sample of approximately 100 x 100 μm, significantly smaller than the spot size of SANS which is typically on the order of 1 cm^2. The reduction in beam size precludes the need to use the entire area of a mask for a single repeating pattern, allowing a variation of pattern sizes and forms. SANS was performed at the NIST Center for Neutron Research using a wavelength of 0.6 nm. Further details of the SANS measurements are provided in a prior publication.[15]

While many materials are inherently transparent to neutrons, the attenuation length (proportional to the inverse of absorption) of x-rays is a significant factor in SAXS measurements. The attenuation length increases as the incident wavelength is decreased for sub-nanomter wavelengths. However, decreasing wavelength has the undesirable effect of decreased resolution, Δq (approximated using $\Delta q/q=((\Delta\lambda/\lambda)^2+(\Delta\theta/\theta)^2)^{1/2}$). As a compromise, a sub-Angstrom wavelength of λ=0.095 nm (13 keV) is chosen, resulting in a ratio of transmitted to incident intensity of 0.10. Losses in resolution due to small λ are overcome, in part, through reductions in $\Delta\lambda$. In contrast to SANS, the comparatively large intensity of x-ray sources allows the use of highly monochromatic beams, providing a wavelength distribution ($\Delta\lambda/\lambda \approx 3 \times 10^{-5}$) several orders smaller than typically used in SANS ($\Delta\lambda/\lambda$=0.11).

3. RESULTS

The dramatic difference in the signal-to-noise ratio (S/N) of SAXS and SANS is demonstrated in figure 3, where the 2-dimensional detector images from sample C are compared. While possessing nearly 4 orders of magnitude smaller beam

area, the SAXS diffraction peak intensity exceeds the background intensity by several orders of magnitude. Further refinement of the x-ray optics, resulting in increased levels of transmitted intensity, would further increase the S/N of the SAXS technique. In both cases, the collection time was approximately 10 min, however SAXS data of adequate quality are readily obtained after several seconds. The ability of small angle scattering to resolve details of pattern quality and line shape is dependent on the number of observable peaks. A poor wavelength resolution results in the loss of higher order peaks as demonstrated in figure 4. Monochromation of the x-ray beam provides more than twofold increase in the resolvable diffraction peaks from the same sample. In addition, the small wavelength spread of SAXS results in a relatively constant resolution over the observable range of q. Given the current level of resolution, SANS is incapable of resolving peaks occurring beyond $q = 0.01$ Å^{-1}.

Given the 1-dimensional symmetry of the patterns, the diffraction axis is similarly 1-dimensional and subsequent analysis is restricted to I(q), where q represents the scattering vectors along the diffraction axis. The total intensity is then written as the squared product of the form factor P(q), describing the average line shape, and the structure factor S(q), representing the relative positions of the lines to each other. With a pattern possessing long range order, S(q) is approximated as a series of delta functions occurring at $q=n2\pi/L$, where L is the average pitch and n is the order of diffraction. The value of L is then extracted in figure 5 using a linear fit of the q values of maximum intensity for each peak from each data set, and assigning an order of diffraction. For sample C, the analysis results in estimates for $L = [543.5 \pm 1.5]$ nm from SAXS and $L = [546.0 \pm 9.1]$ nm from SANS. The larger error in the SANS measurement is due to both error in the estimation of the peaks, especially at higher orders, and the small number of data points in the linear fit. SAXS results from samples A and B result in $L = [553 \pm 1.8]$ and $[550 \pm 2.2]$ nm, respectively.

In addition to periodicity, the average line width is readily obtained by comparing the relative intensities of the peaks. Based on the relationship, $I(q) = |S(q)*P(q)|^2$, the intensities of the peaks follow an "envelope" of the form P(q). In figure 6, the reproducibility of peak position is shown between samples, and is consistent with the use of the same mask. The relative intensities, however, vary dramatically between patterns, suggesting variations in linewidth due to processing conditions or material factors in the resists. To determine an average line width, we employ the form factor of a single line, $P(q) = A \sin(qd/2)/q$, where d is the average line width and A is an arbitrary constant. A fit of the form factor, multiplied by S(q) as determined by the linear fit above, results in a line width of sample C of $[167 \pm 0.9]$ nm (see figure 7). A similar fit of SANS data results in $d = [171 \pm 4.2]$ nm. As with the line periodicity estimate, significant error is incurred in the case of the SANS measurement due to the presence of only two oscillations in P(q). SAXS results provide similar levels of resolution for samples A and B, with $d = [171 \pm 1.2]$ and $[159 \pm 1.6]$ nm respectively.

Finally, we compare these scattering based measurements relative to initial results from real space measurements with AFM. Relatively large errors in the values arise due to the difficulty of insertion of the tip within the narrow line spacings. Future measurements will include substantial increases in AFM precision using ultrasharp tips and calibrated AFM described elsewhere.[18] Here, initial data is provided for sample A here using a conventional AFM calibrated at significantly larger length scales using a standard pitch grating. In figure 8, the values of periodicity, or pitch, and line width are directly compared between the original estimate based on the mask and measurements by SAXS, SANS, and AFM (for sample A only).

4. DISCUSSION

The use of sub-nanometer wavelengths provides many advantages for pattern metrology, including simplified data analysis, however the use of a neutron source in prior studies creates substantial limitations to actual processing environments. Using many of the same principles, these limitations are addressed here using an x-ray source. The large signal above background and the capability to measure high orders of diffraction, increases the information content from a single measurement. For simple qualitative determinations, a series of detector images taken from a dose-matrix of the same mask on the same resist materials are sufficient to locate optimal imaging conditions. This level of analysis can be performed without significant data reduction and manipulation, satisfying the requirement of rapid measurement.

A primary requirement for needed metrology techniques is sub-nanometer resolution. The periodicity from SAXS already displays nanometer precision for the A and B samples, with sub-nanometer resolution for the C sample. Continuing increases in precision will result from increases in instrumental resolution, most easily attained through

continued reduction of the beam size. In addition to increased precision of current data, detailed descriptions of line shape, including parameters such as line height and sidewall angle, are possible with additional measurements. As an example, varying sample orientation can provide a more complete 3-dimensional representation of the average line shape. Further information on the distribution of both pitch and line width are accessible through analysis of peak widths. Additional parameters, such as line height, can be determined for data reduced to absolute intensity.

The application of SAXS is demonstrated here using patterns from a 248 nm exposure system. As semiconductor technology proceeds through the 193 nm node and on to 157 nm and EUV processing, structure sizes will continue to shrink well into the sub-100 nm regime, where EUV lithography may produce structures with critical dimensions less than 50 nm. The reduction of feature size incurs a broadening of the form factor, P(q), and increased peak spacing for S(q). The limits of the technique are then based on the maximum q vector at which peaks are resolved. As we have demonstrated here, resolution smearing is nearly constant across a wide range of q when $\Delta\lambda/\lambda << \Delta\theta/\theta$. If peak smearing is not a substantial effect, then the natural decay of peaks into the background will determine the measurable limit, where the decay rate is dependent on pattern quality. High quality patterns will retain diffraction orders at larger q vectors, while an increased number of defects or lack of long-range order will hasten the drop below background levels.

The transmission geometry of the technique is critical to its extension to embedded, 3-dimensional structures. Because the x-rays pass through the entire sample, depth of penetration is larger than any structure within the sample. However, the available materials for measurement only require measurable differences in electron density between the material and the surrounding matrix. For surface patterns, the data here show that the differences in electron density of low-density organic materials, such as a photoresist, and air or vacuum are suitable for routine measurement. Buried structures, such as in copper interconnects, are feasible given a surrounding matrix of disparate electron density. This generality of materials allows the application of this technique to a wide range of nano-structured and nano-patterned materials.

A final requirement involves portability to a fabrication environment. In this study, a synchotron source provides the appropriate wavelength and optical controls, however the use of a synchotron is not technically required. Given an appropriate source of x-rays with sub-Angstrom wavelengths and appropriate optics for collimation, monochromation, and detection of that wavelength, a laboratory scale device is feasible. For different wavelengths, the compromise of attenuation length, flux, and resolution would require evaluation based on each instrumental factor. Future investigations will explore these requirements.

5. CONCLUSIONS

In conclusion, we have demonstrated the capability of small angle x-ray scattering (SAXS) as a viable measurement tool for pattern characterization in sub-100 nm lithographic processing. The SAXS technique is applicable for both organic systems, such as in photoresists, and inorganic semiconductor structures. Direct comparison with small angle neutron scattering (SANS), shows a dramatic increase in precision. This increased precision is due to a larger signal-to-noise ratio and better instrumental resolution at high q vectors. SAXS currently provides nanometer level resolution, however the precision is readily extended to sub-nanometer levels with adjustments of the x-ray optics. Measurement time, on the order of seconds, and measurement probe size, on the order of 100 μm, are both comparable to light scatterometry. While this study is performed using a synchotron x-ray source, a laboratory-based device of similar capabilities is technically feasible with appropriate optical components.

ACKNOWLEDGEMENTS

This work was funded in part by the DARPA Advanced Lithography Program under contract N66001-00-C-8803. Additional funding was provided by the NIST Office of Microelectronic Programs. The Advanced Photon Source and D. M. C. are supported by the U.S. Department of Energy under contract no. W-31-109-Eng-38. R. L. J. is supported by a NIST National Research Council postdoctoral fellowship.

REFERENCES

1. J. S. Villarrubia, R. Dixson, S. Jones, J.R. Lowney, M. T. Postek, R. A. Allen, and M. W. Cresswell, "Intercomparison of SEM, AFM, and Electrical Linewidths", *Proc.of SPIE: Metrology, Inspection, and Process Control for Microlithography XIII* **3677**, 587-598, Santa Clara, 1999.
2. Y. Ose, M. Ezumi, T. Ishijima, H. Todokoro, and K. Nagai, "Correction Method for High-Precision CD-Measurements on Electrostatically Charged Wafers", *Proc.of SPIE: Metrology, Inspection, and Process Control for Microlithography XVI* **4689**, 128-137, Santa Clara, 2002.
3. B. D. Bunday and M. Bishop, "Benchmarking of Advanced CD-SEMs at the 130nm CMOS Technology Node", *Proc.of SPIE: Metrology, Inspection, and Process Control for Microlithography XVI* **4689**, 102-115, Santa Clara, 2002.
4. H. M. Marchman, J. E. Griffith, J. Z. Y. Guo, J. Frackoviak, and G. K. Celler "Nanometer-scale dimensional metrology for advanced lithography", *J. Vac. Sci. Technol. B* **12**, 3585-3590, 1994.
5. C. J. Raymond, M. R. Murnane, S. L. Prins, S. Sohail, H. Naqvi, and J. R. McNeil "Multiparameter grating metrology using optical scatterometry", *J. Vac. Sci. Technol. B* **15**, 361-368, 1997.
6. V. Machavariani, S. Gov, and Y. Cohen "Scatterometry – interpretation by different methods of electromagnetic simulation", *Proc. of SPIE: Metrology, Inspection, and Process Control for Microlithography XVI* **4689**, 177-188, 2002.
7. S. K. Sinha, "The impact of synchotron radiation on nanoscience", *Appl. Surf. Sci.* **182**, 176-185, 2001.
8. P. Mikulik and T. Baumbach, "X-ray reflection by multilayer surface gratings", *Physica B* **248**, 381-386, 1998.
9. G. T. Baumbach, D. Lubbert, U. Pietsch, N. Darowski, L. Leprince, A. Talneau, and J. Schneck "Grazing incidence diffraction by epitaxial multilayer gratings", *Physica B* **248**, 343-348, 1998.
10. M. Tolan, W. Press, F. Brinkop, and J.P. Kotthaus "X-ray diffraction from laterally structured surfaces: Total external reflection", *Phys. Rev. B* **51**, 2239-2251, 1995.
11. V. Holy, J. Stangl, G. Springholz, M. Pinczolits, and G. Bauer "High-resolution x-ray diffraction from self-organized PbSe/PbEuTe quantum superlattices", *J. Phys. D. Appl. Phys.* **34**, A1-A5, 2001.
12. P. van der Sluis, J. J. M. Binsma, and T. van Dongen, "High resolution x-ray diffraction of periodic surface gratings", *Appl. Phys. Lett.*, **62**, 3186-3188, 1993.
13. Q. Shen, C. C. Umbach, B. Weselak, and J. M. Blakely, "X-ray diffraction from a coherently illuminated Si(001) grating surface", *Phys. Rev. B* **48**, 17967-17971, 1993.
14. A. T. Macrander and S. E. G. Slusky, "X-ray diffraction from corrugated crystalline surfaces and interfaces", *Appl. Phys. Lett.* **56**, 443-445, 1990.
15. The data in this manuscript, in the figures, and in the tables are presented along with the standard uncertainty (±) involved in the measurement, where the uncertainty represents one standard deviation from the mean.
16. E. K. Lin, R. L. Jones, W.-L. Wu, J. G. Barker, P. J. Bolton, and G. G. Barclay, *Proc.of SPIE: Metrology, Inspection, and Process Control for Microlithography XVI*, **4689**, 541-548, Santa Clara, 2002.
17. R. Dixson, N. G. Orji, J. Fu, V. Tsai, E. D. Williams, R. Kacker, T. Vorburger, H. Edwards, D. Cook, P. West, and R. Nyffenegger "Silicon single atom steps as AFM height standards", *Proc. of SPIE: Metrology, Inspection, and Process Control for Microlithography XV*, **4344**, 157-168, 2001.
18. E. K. Lin, C. L. Soles, D. L. Goldfarb, B. C. Trinque, S. D. Burns, R. L. Jones, J. L. Lenhart, M. Angelopoulos, C. G. Willson, S. K. Satija, and W.-l. Wu "Reaction front in chemically amplified photoresists", *Science* **297**, 372-375, 2002.

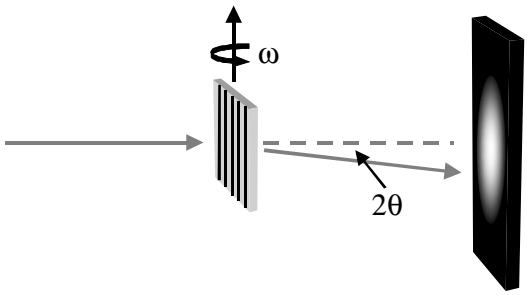

Figure 1. Schematic of SAXS and SANS geometry. The beam (grey line) is shown relative to the sample and the detector, illustrating the scattering angle, 2θ, relative to the unscattered beam (dashed grey line). Rotation of the pattern is accomplished by sample rotation about a separate axis, ω.

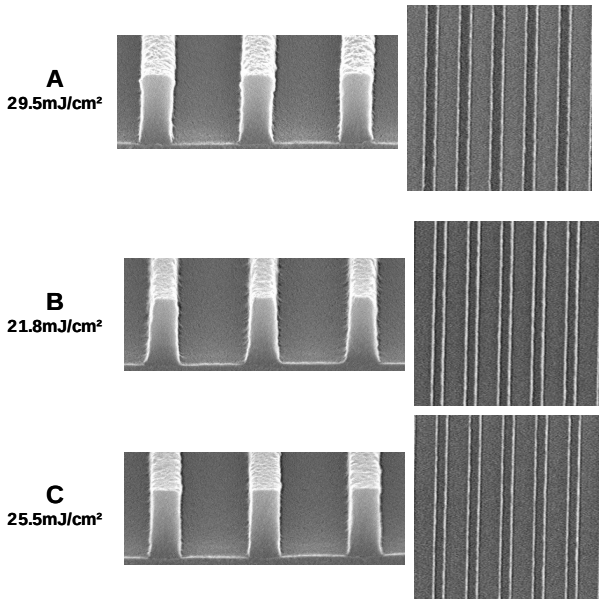

Figure 2. SEM image of photoresist gratings used in this study. Shown are samples A, B, and C in cross section (left) and top-down views (right).

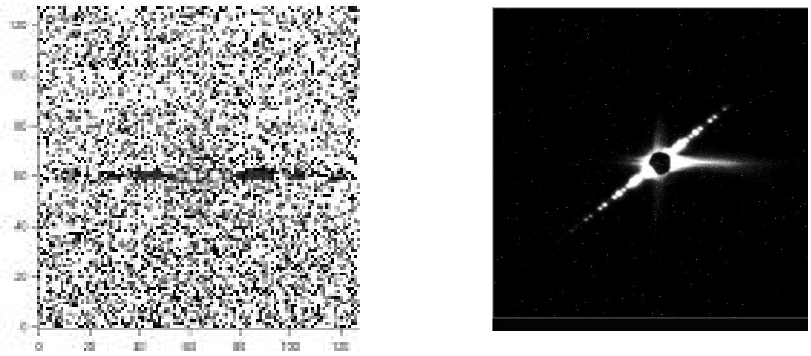

Figure 3. Comparison of 2-d images collected for sample C using (a) SANS and (b) SAXS. For SANS, diffraction peaks are barely visible along a horizontal diffraction axis, while the SAXS data along an axis approximately 45º to the horizontal are clearly observed above the background. SAXS image also features slit scattering observed along the horizontal and vertical axis.

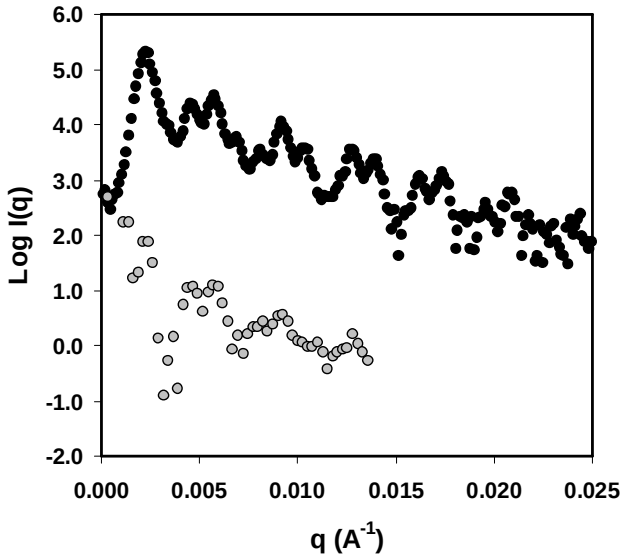

Figure 4. Scattered intensity as a function of q plotted for sample C from (a) SANS and (b) SAXS. Intensities are not on absolute scale.

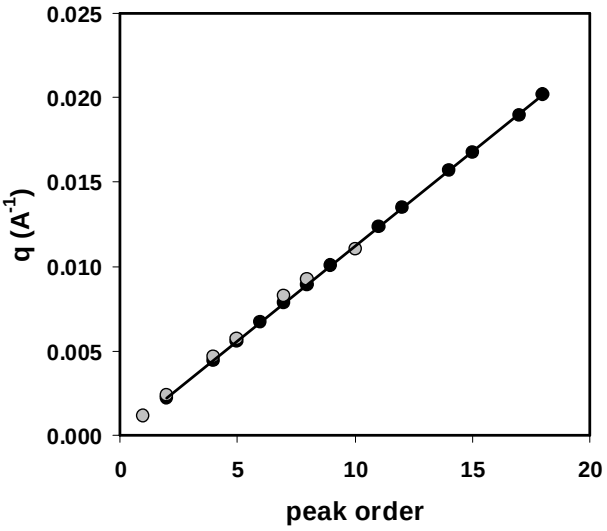

Figure 5. Position along q_x of maximum intensities of each peak plotted as a function of the diffraction order. Shown are data from sample C resulting from SANS (grayed circles) and SAXS (solid circles) data, along with a linear fit to the SAXS data (solid lines).

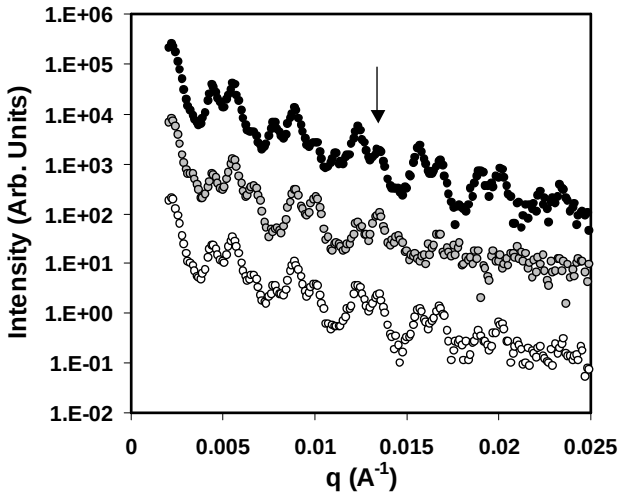

Figure 6. Scattered intensity from SAXS as a function of q plotted for samples A (solid circles), B (grayed circles), and C (open circles). The relative intensities are shown to vary between samples as illustrated by the 12^{th} order highlighted by the arrow.

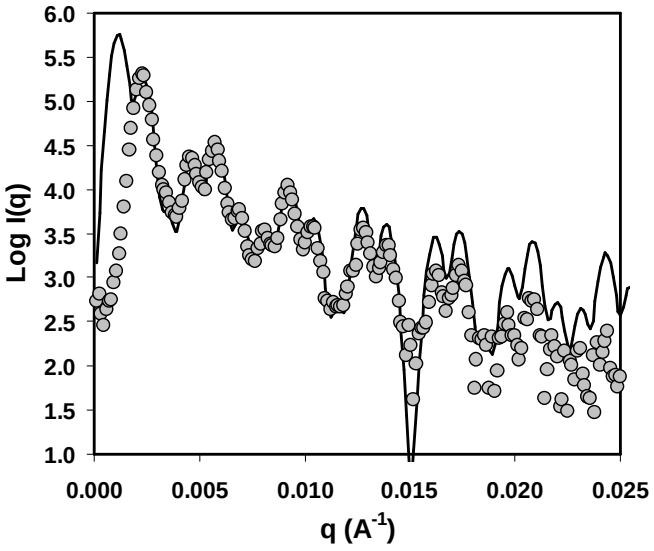

Figure 7. Logarithm of Intensity as a function of q. Plotted are data from SAXS measurements of sample C along with a simple fit using model described in text.

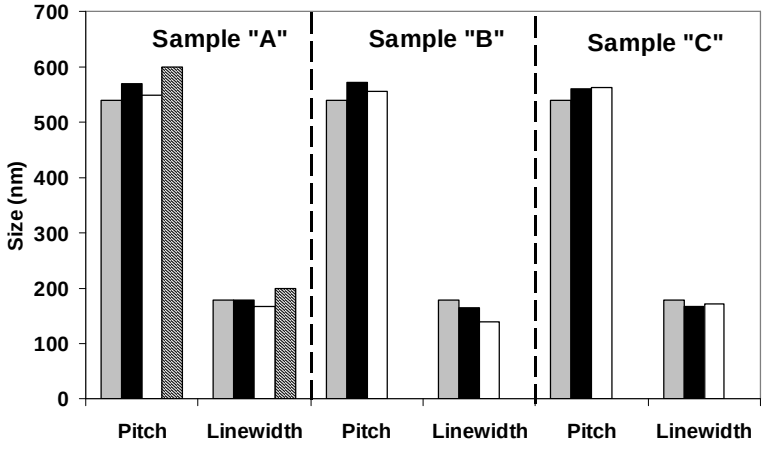

Figure 8. Values obtained from SANS and SAXS for basic pattern quality including periodicity and line width. Shown are values for the nominal estimate from the mask (grey), and values obtained from SANS (black) and SAXS (white). For sample A, additional values are given using AFM (hatched). Uncertainty in the AFM values is estimated as no more than 10% of the value.